Article

Structure

Crystal Structure of Green Fluorescent Protein Clover and Design of Clover-Based Redox Sensors

Graphical Abstract

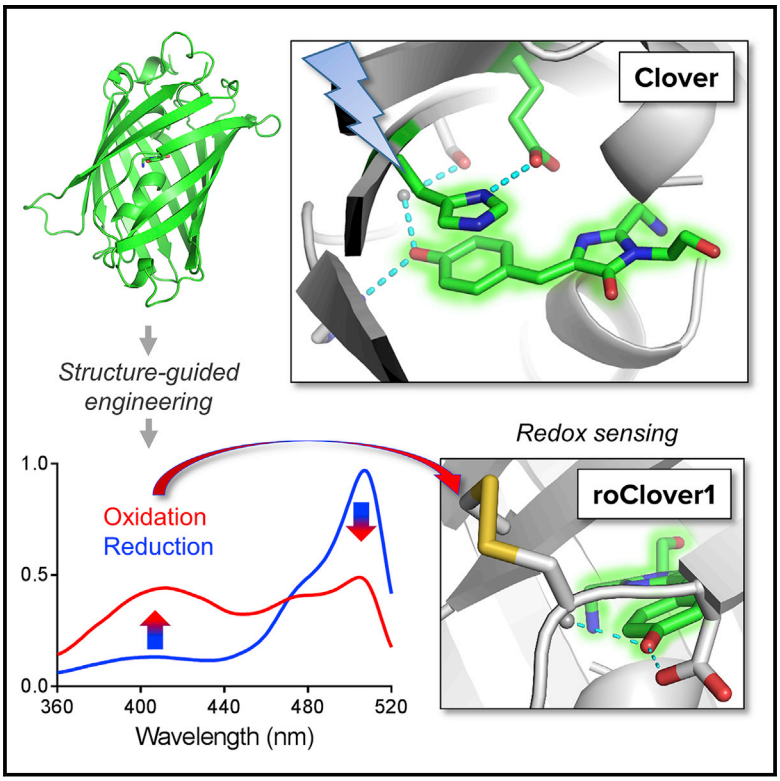

Highlights

- In contrast to PA-GFP, Clover's T203H mutation strengthens the anionic chromophore
- An H203-E222 interaction contributes to Clover's large extinction coefficient
- roClover1 is an excitation-ratiometric redox sensor using a new proton acceptor
- Non-photoactivatable GFP-based biosensors can be engineered in the protonated form

Authors

Benjamin C. Campbell, Gregory A. Petsko, Ce Feng Liu

Correspondence

cel2010@med.cornell.edu

In Brief

Campbell et al. solve the crystal structure of Clover, one of the brightest fluorescent proteins, and describe its structure-function relationships. Using these data, they engineer and crystallize mutants that respond to oxidation and reduction. The structures of Clover, roClover0.1, and roClover1 offer strategies and templates for GFP-based biosensor design.

Campbell et al., 2018, Structure *26*, 225–237
February 6, 2018
https://doi.org/10.1016/j.str.2017.12.006

CellPress

Structure
Article

Crystal Structure of Green Fluorescent Protein Clover and Design of Clover-Based Redox Sensors

Benjamin C. Campbell,[1] Gregory A. Petsko,[1] and Ce Feng Liu[1,2,*]
[1]Helen and Robert Appel Alzheimer's Disease Research Institute and Feil Family Brain and Mind Research Institute, Weill Cornell Medicine, New York, NY 10021, USA
[2]Lead Contact
*Correspondence: cel2010@med.cornell.edu
https://doi.org/10.1016/j.str.2017.12.006

SUMMARY

We have determined the crystal structure of Clover, one of the brightest fluorescent proteins, and found that its T203H/S65G mutations relative to wild-type GFP lock the critical E222 side chain in a fixed configuration that mimics the major conformer of that in EGFP. The resulting equilibrium shift to the predominantly deprotonated chromophore increases the extinction coefficient (EC), opposes photoactivation, and is responsible for the bathochromic shift. Clover's brightness can further be attributed to a π-π stacking interaction between H203 and the chromophore. Consistent with these observations, the Clover G65S mutant reversed the equilibrium shift, dramatically decreased the EC, and made Clover photoactivatable under conditions that activated photoactivatable GFP. Using the Clover structure, we rationally engineered a non-photoactivatable redox sensor, roClover1, and determined its structure as well as that of its parental template, roClover0.1. These high-resolution structures provide deeper insights into structure-function relationships in GFPs and may aid the development of excitation-improved ratiometric biosensors.

INTRODUCTION

The green fluorescent protein (GFP) derived from crystal jelly *Aequorea victoria* rapidly became an indispensable tool in biology after its use as a genetically encodable marker for gene expression studies in *Caenorhabditis elegans* over two decades ago (Chalfie et al., 1994). The improved folding and brightness of enhanced GFP (EGFP) secured its place as a reliable and versatile tag for gene expression, and to this day it remains the standard against which all fluorescent proteins (FPs) are compared.

The excitation spectrum of wild-type GFP (wtGFP) consists of a major ~400 nm peak (A band) and a minor ~480 nm peak (B band), corresponding to the neutral and anionic chromophore species, respectively (Meech, 2009). Excitation of the A band results in fast excited-state proton transfer (ESPT) from the chromophore's phenol moiety to the acidic E222, generating an anionic intermediate I* state that decays radiatively with emission of a green photon (Henderson et al., 2009a; Jung et al., 2005; Meech, 2009). Excitation of the B band results in direct green emission, and the amplitude of these excitation peaks changes inversely depending on the equilibrium between the neutral and the anionic chromophore, which can be modified through environmental or structural perturbations.

The redox-sensitive GFPs (roGFPs) harness these photophysical properties to function as excitation-ratiometric biosensors (Hanson et al., 2004). Upon oxidation, an engineered cysteine pair (S147C-Q204C) located on adjacent β strands of the protein's antiparallel sheet barrel structure forms a disulfide bond that introduces local geometric strain into a flexible region of the barrel and modifies the chromophore protonation equilibrium. The resulting shift in the ratio of neutral to anionic chromophores produces a corresponding change in the excitation spectrum that allows the proteins to serve as quantitative biosensors through excitation ratiometry (Dooley et al., 2004; Hanson et al., 2004). Despite their widespread use in numerous model organisms and versatility as genetically encoded probes, all roGFPs are still based on wtGFP and EGFP, so they inherit those proteins' disadvantages, particularly irreversible redox-independent photoactivation that can disrupt long-term measurements (Schwarzländer et al., 2008).

We sought to develop a non-photoactivatable redox sensor using Clover (Lam et al., 2012), one of the brightest FPs engineered to date (Thorn, 2017), as a template for structure-guided engineering. Clover incorporates most of the superfolder GFP (sfGFP) mutations (Pédelacq et al., 2006) and differs from sfGFP by L64F/T65G/Q69A/T203H/V206A (Table S1). Although Clover shares the critical T203H mutation of photoactivatable GFP (PA-GFP) (Henderson et al., 2009b; Patterson and Lippincott-Schwartz, 2002), Clover does not photoactivate, perhaps due to a lack of the neutral chromophore species (Bajar et al., 2016; Lam et al., 2012).

We determined the crystal structure of Clover (to 2.4 Å resolution) and found that the T203H/S65G mutations relative to wtGFP lock the critical E222 side chain in a configuration similar to that of the major conformer in EGFP, stabilizing the anionic chromophore. The resulting equilibrium shift increases the extinction coefficient (EC), opposes photoactivation, and produces the bathochromic shift. In addition, a π-π stacking interaction between H203 and the chromophore phenolate improves chromophore packing and limits non-radiative decay of the excited state, thereby increasing quantum yield. Introducing mutation G65S reversed the equilibrium shift, dramatically decreased the EC, and enabled photoactivation under

Table 1. Crystallographic Data Refinement and Statistics

	Clover	roClover0.1	roClover1
Resolution range (Å)	43.5–2.40	46.0–1.35	39.2–1.63
Space group	I222	$P2_12_12_1$	$P4_32_12$
Cell dimensions			
a (Å)	53.1	68.6	134.6
b (Å)	135.2	82.0	134.6
c (Å)	168.6	92.0	69.09
Total no. of reflections	1,296,318	1,503,110	1,153,345
No. of unique reflections	23,888	114,122	79,222
Completeness (%)	99.6 (97.0)[a]	97.0 (93.0)[a]	100 (99.9)[a]
Linear R_{merge} (%)[b]	12 (84)[a]	5.2 (46)[a]	11 (51)[a]
I/σ (I)	13 (3.3)[a]	28 (4.8)[a]	11 (1.6)[a]
R_{work}, R_{free} (%)[c]	19.4, 22.4	14.2, 16.4	16.4, 19.3
RMSD for bond length (Å)	0.004	0.005	0.016
RMSD for angle distances (Å)	0.956	1.11	1.37
Average B ($Å^2$)	54.1	20.8	32.1
Ramachandran plot (%)			
Favored	98.2	98.9	99.1
Allowed	1.6	1.1	0.88
PDB ID	5WJ2	5WJ3	5WJ4

$R_{work} = \Sigma|F_{obs} - F_{calc}|/F_{calc}$. All reflections except the test set were used to calculate R_{work}.

[a]Statistics in parentheses correspond to data in the highest resolution bin (2.52–2.40 Å for Clover, 1.37–1.35 Å for roClover0.1, and 1.65–1.63 Å for roClover1).

[b]$R_{merge} = \Sigma|I_{obs} - I_{avg}|/I_{avg}$.

[c]$R_{free} = \Sigma|F_{obs} - F_{calc}|/F_{calc}$. Five percent of the total reflections were chosen at random as the test set, and only the test set was used to calculate R_{free}.

conditions that activated PA-GFP and roGFP1. Using the Clover structure, we rationally engineered a non-photoactivatable redox-sensitive mutant, roClover1, and determined its structure (1.6 Å resolution), along with that of its parental template, roClover0.1 (1.3 Å resolution), which featured a larger quantum yield than Clover. These high-resolution structures provide deeper insight into structure-function relationships in GFPs and may aid development of optical highlighters and excitation-ratiometric biosensors.

RESULTS

General Structural Features of Clover

Clover crystallized with the symmetry of space group I222, diffracted to 2.4 Å resolution, and the structure was solved by molecular replacement using a homology model generated from an EGFP mutant (PDB: 1QYQ; Barondeau et al., 2003). Two molecules of Clover were found in the asymmetric unit and the root-mean-square deviation (RMSD) between these two molecules was 0.19 Å (Table 1). The overall structure of Clover is very similar to those of other FPs derived from *A. victoria* (avFPs) (Figure 1). It has the canonical 11-stranded β barrel motif with the chromophore tucked inside the core of the barrel. The RMSD of Clover to the high-resolution structures of EGFP with codes PDB: 4EUL and 2Y0G is 0.33 and 0.35 Å, respectively. Compared with wtGFP, Clover has 11 mutations, eight of which are derived from sfGFP (Pédelacq et al., 2006). In our Clover structure, these eight mutations (S30R, Y39N, F99S, N105T, Y145F, M153T, V163A, and I171V) are predominantly far from the chromophore and the specific interactions said to increase folding of sfGFP as a result of these mutations have remained intact.

Clover's chromophore is shifted 0.6–0.7 Å toward β strands 7 and 8 compared with EGFP (PDB: 2Y0G) (Figure 1C) and sfGFP (PDB: 2B3P), inducing a minor compensatory displacement of strand 8, which leaves the distances between the chromophore and the neighboring residues such as H148, F165, and I167 unchanged. The shift in chromophore position can be attributed to the T65G substitution and a π-π orbital stacking interaction of the chromophore with the aromatic ring of H203. Attraction of the chromophore toward H203 on strand 10 and elimination of the hydrogen-bond (H-bond) interaction that normally exists between T65 and E222 on strand 11 has repositioned the chromophore toward neighboring strands 7 and 8.

π-π Stacking Interaction Contributes to the Bathochromic Shift of Clover

The mentioned π-π stacking interaction between H203 and the Clover chromophore is similar to that of on-state PA-GFP ($PA\text{-}GFP_{on}$) (Figure 1D) and diverse red-shifted FPs such as zFP538 (Remington et al., 2005) and mRuby (*cis* conformation) (Kredel et al., 2009), all of which feature a histidine at the equivalent position by structure alignment. Clover and $PA\text{-}GFP_{on}$ have similar excitation and emission maxima and quantum yields (ϕ = 0.75 versus 0.79, respectively) (Table 2), although Clover's EC is nearly six times greater (111.0 versus 17.4 mM^{-1} cm^{-1}), according to published values (Lam et al., 2012; Patterson and Lippincott-Schwartz, 2002). The distance between the centroids of the H203 imidazole ring and the phenolic ring in Clover is 3.7 Å and the interplanar angle between them is 10.6°. These geometries permit H203 and the chromophore (CRO) to form optimal π-π stacking interactions (Huber et al., 2014) and may contribute to its large quantum yield (QY) through improved chromophore packing.

Features of the Clover Proton Wire that Contribute to Chromophore Deprotonation

Our Clover structure suggests that the H-bond network involving the anionic E222 that stabilizes the neutral chromophore in wtGFP, and is partially disrupted in EGFP due to S65T, is disrupted to a greater extent in Clover, but the effect is mediated through a different set of molecular interactions. High-resolution structures of EGFP reveal that the major E222 conformer (70%) is protonated and neutral, which allows E222 to donate an H bond to T65 (Figure 1B), thereby eliminating the H-bond network that stabilizes the neutral chromophore and shifting the equilibrium toward the anionic form at ~488 nm (Arpino et al., 2012). In Clover, the T65G/T203H substitutions relative to EGFP eliminate H-bond acceptor T65 and enable E222 to donate the H bond to H203 instead, placing E222 $O_{\varepsilon 1}$ 2.7 Å from H203 $N_{\delta 1}$ and 4.3 Å from S205 O_{γ} (Figure 1A). This conformation of

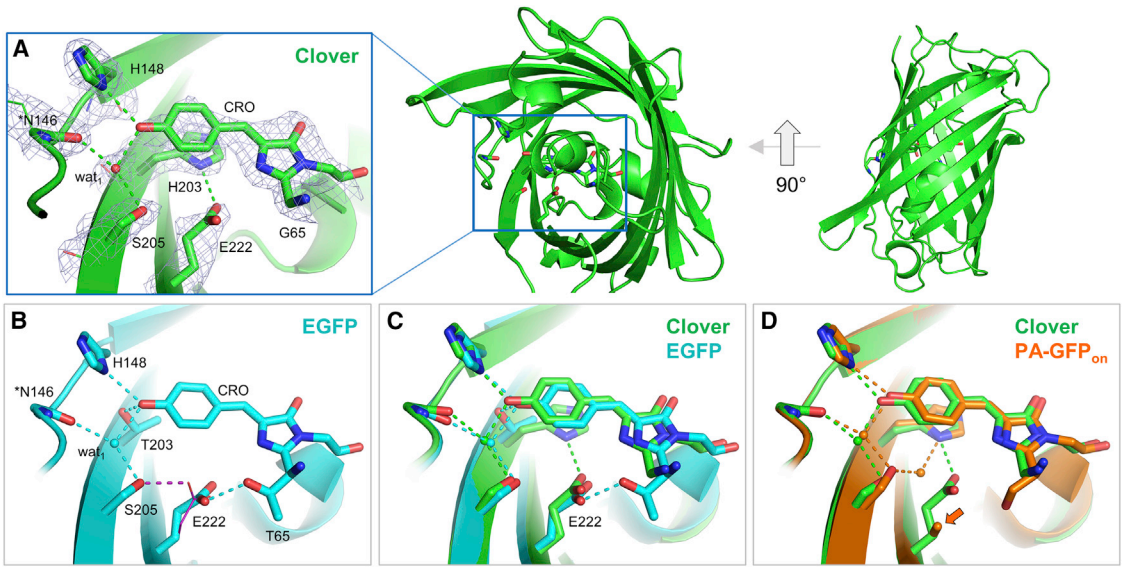

Figure 1. A Hydrogen Bond between Clover H203-E222 Side Chains Locks E222 into a Fixed Configuration that Is Similar to that of the Major Conformer in EGFP

(A) Composite omit map (with simulated annealing) of key residues in the Clover structure, contoured at $\sigma = 1$. Dashes, hydrogen bonds.

(B) In EGFP, E222 adopts two distinct conformations that permit a hydrogen bond between S205 and E222 (30% occupancy, purple line drawing) or E222 and T65 (70%). Asterisk, N146 main chain is displayed with external-facing side chain omitted.

(C) Superposition of the Clover and EGFP structures reveals a similar conformation of E222 (minor EGFP E222 conformer omitted).

(D) Clover and PA-GFP$_{on}$ chromophores are stabilized by hydrogen bonds from wat$_1$ and H148, while the H203 side chain participates in a π-π stacking interaction. Dashes, hydrogen bonds; orange arrow, decarboxylated E222 remnant (Cγ methyl). Clover (PDB: 5WJ2), EGFP (PDB: 2Y0G), PA-GFP$_{on}$ (PDB: 3GJ2).

E222 in Clover, which is the only conformation observed in our structure, also allows E222 to remain protonated and neutral, thereby making chromophore deprotonation in Clover more favorable. Likely as a result of the new H203-E222 H bond and abolition of the T65-E222 H bonds due to G65, the specific conformation of E222 in Clover closely matches the major E222 conformer observed in the high-resolution EGFP structures (PDB: 4EUL and 2Y0G) (Figure 1B). Thus, EGFP and, to a greater extent, Clover strongly favor chromophore deprotonation by maintaining the neutral E222 state and disrupting the wtGFP-like proton wire, but EGFP does it through S65T, and Clover uses S65G/T203H.

Photoactivation and Extinction Coefficient of Clover

Consistent with the assertion that S65G/T203H mutations in Clover greatly favored the deprotonated chromophore, mutating G65 to S65 to produce Clover-G65S restored the 400 nm A band while nearly eliminating the B band (Figure 2B). We successfully photoactivated PA-GFP and Clover-G65S under identical illumination conditions, resulting in activation contrast of 10- and 2-fold, respectively, whereas Clover^{wt} showed a reduction in B-band absorbance, likely due to mild photobleaching only (Figures 2C–2E). Interestingly, the pre-exposure B-band absorbance of Clover-G65S$_{off}$ was 5-fold larger than that of PA-GFP$_{off}$, although the 400 nm peak was still 10 times larger than the B band (Figures 2D and 2E), indicating a mostly neutral chromophore.

We used the alkali denaturation method (Cranfill et al., 2016) to determine the ECs of Clover-G65S$_{off}$ and PA-GFP$_{off}$ and found that the EC of the Clover-G65S$_{off}$ B band was smaller than that of Clover^{wt} by a factor of 39 (2,500 M^{-1} cm^{-1} versus 98,000 M^{-1} cm^{-1}) (Table 2). The EC of the PA-GFP$_{off}$ B band was too small to calculate with confidence (<1,000 M^{-1} cm^{-1}), although the EC of the A band was identical for both proteins at 34,000 M^{-1} cm^{-1} at 400 nm. We chose not to calculate the on-state ECs at any wavelength because we were unable to photoactivate the proteins to completion using our light source (at least 80-fold contrast would be necessary for PA-GFP$_{on}$) (Patterson and Lippincott-Schwartz, 2002). The susceptibility of Clover-G65S to photoactivation further demonstrates the importance of chromophore deprotonation in Clover^{wt} for opposing it.

Modifications that shift the equilibrium from the neutral to the anionic chromophore would increase the fluorophore's EC at the anionic chromophore absorbance peak and vice versa. We experimentally confirmed the EC of EGFP, sfGFP, and Clover (Table 2), and our results align with those recently reported (Cranfill et al., 2016). Clover's EC is nearly twice as high as EGFP's (98,000 versus 54,000 M^{-1} cm^{-1}, respectively). With its equilibrium shifted further toward the anionic species, Clover is able to absorb, and with its higher QY, convert more light than EGFP when excited at its anionic absorbance peak.

Bathochromic Shift of Clover

Since planarity of the chromophore and QY are positively correlated (Bindels et al., 2016; Chu et al., 2016; Subach and Verkhusha, 2012), we compared the planarity of the Clover chromophore with that of EGFP and sfGFP, but observed no significant differences (Table S2), suggesting that other factors are more important for determining the brightness of Clover. We note that the asymmetric ring stacking between H203 and the

Table 2. Spectral Properties of Fluorescent Proteins Discussed in This Study

Protein	λ_{ex}[a] A	λ_{ex}[a] B	λ_{em}[b] A	λ_{em}[b] B	pK_a	ϕ	ε[c]	Primary Reference
EGFP	–	488	–	507	6.0	0.60	54,000	Sarkisyan et al., 2015
Superfolder GFP	–	485	–	510	–	0.65	52,000	Pédelacq et al., 2006
PA-GFP$_{off}$	–	–	–	–	–	0.13	<1,000	Patterson and Lippincott-Schwartz, 2002
PA-GFP$_{on}$	–	504	–	517	–	0.79	[d]	Patterson and Lippincott-Schwartz, 2002
Clover-G65S$_{off}$	–	–	–	–	–	–	2,500	this work
Clover-G65S$_{on}$	–	–	–	–	–	–	[d]	this work
Clover	–	505	–	515	6.1	0.75[c]	98,000	Lam et al., 2012
roClover0.1$_{ox}$	–	–	–	–	–	0.79	96,000	this work
roClover0.1$_{rd}$	–	507	–	516	–	0.75	86,600	this work
roClover0.2	384	457	450	520	–	–	–	this work
roClover0.3	–	503	–	513	–	–	–	this work
roClover1$_{ox}$	409	505	454/505	510	>9.0	0.01	10,600	this work
roClover1$_{rd}$	409	507	454/500	515	>9.0	0.02	7,300	this work
GFP-S65G/H203V/E222Q	395	500	450/513	513	–	0.18	13,300[e,f]	Jung et al., 2005
GFP-S65T/H148D	415	487	510	510	8.0	–	–	Shu et al., 2007a
roGFP1$_{ox}$	390	475	508	508	–	0.40[c]	6,200	Hanson et al., 2004
roGFP1$_{rd}$	390	475	508	508	–	0.71[c]	9,600	Hanson et al., 2004
roGFP2$_{ox}$	400	495	509	509	6.0	0.61[c]	23,100	Hanson et al., 2004
roGFP2$_{rd}$	400	490	509	509	5.6	0.67[c]	50,600	Hanson et al., 2004

Dash indicates "value absent," "not determined," or "not applicable."
[a]Excitation maximum in nanometers.
[b]Emission maximum in nanometers after excitation of the neutral (A-state) or anionic (B-state) chromophore.
[c]Experimentally determined in our lab. All values are for the anionic chromophore unless otherwise indicated.
[d]We did not determine these values because photoactivation was not performed to completion.
[e]Cited from primary reference.
[f]Extinction coefficient reported for absorbance maximum of A band rather than B band.

Clover chromophore does not lead to the formation of a centrosymmetric inversion center such as that found in EYFP (PDB: 1YFP), which has been suspected to limit the EYFP QY (De Meulenaere et al., 2013) (Figure S1A). Clover's H203 is shifted off-center relative to the chromophore phenolate moiety by approximately 1 Å (Figure S1B) toward V150. Lack of centroid-to-centroid alignment in H203 mutants is a common feature of the histidine stacking interaction in diverse FPs, including PA-GFP$_{on}$ (*A. victoria*), mTFP1 (*Clavularia* sp.), and zFP538 (*Zoanthus* sp.) (Figure S1C). In addition to improving brightness, these stacking interactions tend to red-shift fluorescence spectra by expanding the chromophore's π-electron cloud and decreasing the energetic gap between the ground and the excited states, similar to the effect of T203Y in YFPs (Wachter et al., 1998). The fluorescence spectra of Clover and PA-GFP$_{on}$ are red shifted by ~20 nm compared with those of EGFP and sfGFP (Table 2) due to the T203H mutation.

Development of Redox-Sensitive Clover Mutants

To generate a redox sensor resistant to photoactivation, we selected Clover as a template for structure-guided engineering and applied the S147C and Q204C mutations, resulting in roClover0.1. Whereas those two mutations were sufficient to produce an excitation-ratiometric roFP from EGFP (roGFP2) (Hanson et al., 2004), roClover0.1 was hardly redox sensitive when exposed to the oxidizer 2,2-dipyridyl disulfide (DPS) or the reductant dithiothreitol (DTT) (Figure 3B). Under identical experimental conditions, 2 mM DPS or 5 mM DTT fully oxidized and reduced roGFP2, respectively (Figure 3F), yielding an average dynamic range of 6.0, similar to the reported literature value of 5.8 (Hanson et al., 2004).

We suspected that Clover's strongly deprotonated chromophore might account for the lack of responses to C147-C204 oxidation in roClover0.1, since the wtGFP-like proton wire is disrupted due to the H203-E222 H bond in the Clover crystal structure (Figure 1A). We hypothesized that introducing a new proton acceptor proximal to the chromophore would facilitate responses to C147-C204 oxidation by destabilizing the anionic chromophore and shifting the equilibrium toward the neutral form. In several studies, the H148D substitution has been shown to constitute an alternate proton acceptor that forms a strong H bond with the neutral chromophore phenol to redirect ESPT (Shi et al., 2007; Meech, 2009; Shu et al., 2007a, 2007b), so we applied this mutation to roClover0.1. Indeed, H148D successfully shifted the chromophore equilibrium toward the protonated, neutral chromophore in the resulting mutant, roClover0.2 (Figure 3C). The excitation maxima of roClover0.2 are 384 and 457 nm (Table 2, Figure 3C), in contrast to the single excitation peak of roClover0.1 at 507 nm

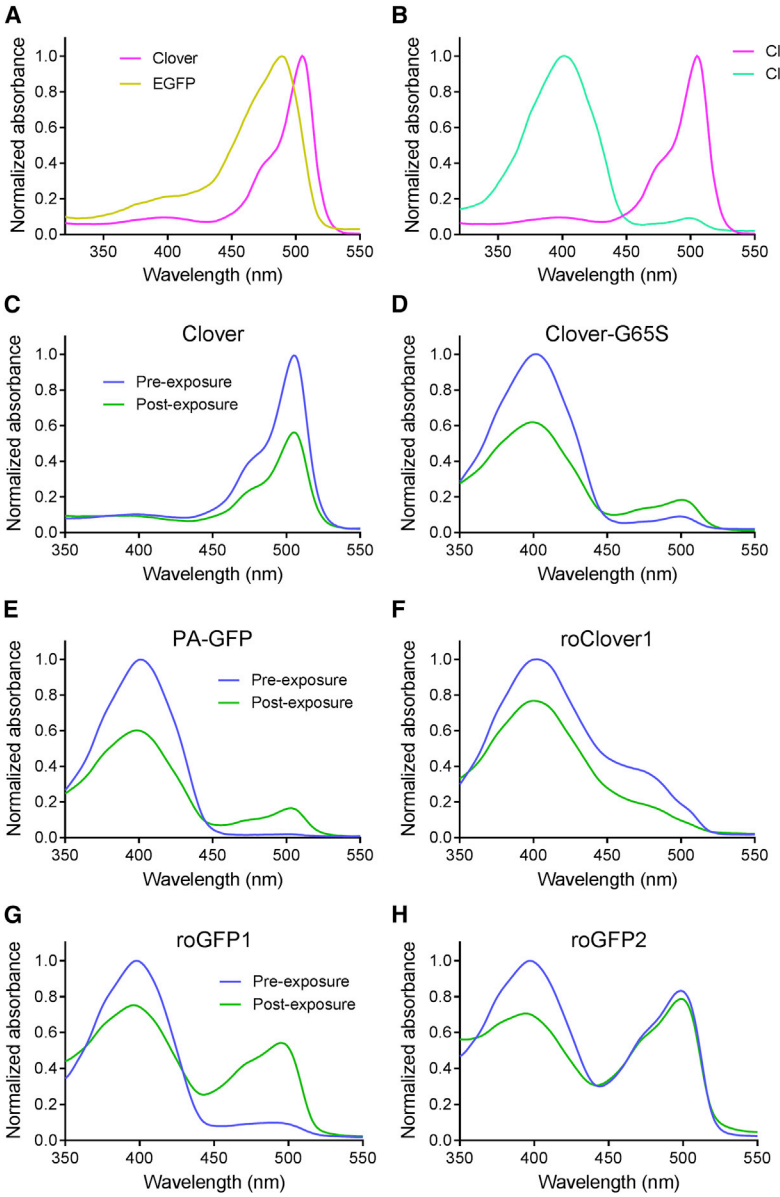

Figure 2. Absorbance Scans of Fluorescent Proteins Before and After Photoactivation

(A) Absorbance scans of Clover and EGFP. Clover has a larger ratio of anionic to neutral chromophore than EGFP, as indicated by Clover's smaller A-band absorbance.

(B) Absorbance scans of Clover and Clover-G65S, which show nearly reciprocal A/B-band ratio.

(C–H) Absorbance scans of fluorescent proteins exposed to 410 nm LED illumination (14 mW/cm^2) for 20 min. Clover (C), roClover1 (F), and roGFP2 (H) mildly bleached but did not photoactivate. PA-GFP (E), Clover-G65S (D), and roGFP1 (G) activated with contrast of 10-, 2-, and 5-fold, respectively.

(Table 2, Figure 3B). Despite the restored A state, roClover0.2 was not clearly redox sensitive, which suggested that structural perturbations induced by oxidation of the C147-C204 pair were still uncoupled to the A-B state equilibrium.

We reasoned that long-range electrostatic effects of E222 in the GFP photocycle (Meech, 2009) might influence proton transfer to H148D and hinder redox responses in roClover0.2. In addition, a study exploring multiple combinations of point mutations at positions 65, 203, and 222 found that S65G/H203V/E222Q effectively shifted the chromophore ionization equilibrium toward the neutral form, resulting in two excitation peaks, whereas S65G/H203V and S65G/E222Q mutants showed only a single peak (Jung et al., 2005). We therefore predicted that the H203V/E222Q combination would be most promising for maintaining the equilibrium shift to the A state observed in roClover0.2, while also disrupting the canonical ESPT pathway and potentially enabling excitation-ratiometric redox responses. We subsequently applied mutations H203V/E222Q to the roClover0.2 template. H203V eliminates the π-π stacking interaction with the chromophore, while E222Q replaces the acidic Glu with Gln so that it can no longer accept a proton or be decarboxylated. The resulting mutant, roClover1 (roClover0.1-H148D/H203V/E222Q), is an excitation-ratiometric roFP with excitation maxima at 409 and 505 nm and a dynamic range of ~6.8 (Figure 3E), slightly greater than that of roGFP2 at pH 7.4 (Figure 3F).

We also applied the H203V/E222Q mutations to the roClover0.1 background (without H148D) to produce roClover0.3, but those mutations were not sufficient to generate a redox-sensitive mutant (Figure 3D). Only the specific combination of mutations in roClover1 yielded an excitation-ratiometric green redox sensor.

Spectral Properties of roClover1 and roGFPs

roClover1 features a prominent absorbance peak at ~400 nm, corresponding to the neutral chromophore, that towers over the minor absorbance shoulders of ~475 and 505 nm in the oxidized and reduced protein, respectively (Figures 4A and 4B). The spectral properties of roClover1 (G65/H203V/E222Q/H148D) are similar to those of the GFP-S65G/H203V/E222Q mutant previously examined (Jung et al., 2005), despite its additional H148D mutation. roClover1 displays blue and green emission after excitation at 390 nm and green emission after 460 nm excitation and features a small absorbance peak around 505 nm.

The spectral properties of roClover1 depended on the presence of oxidant and reductant and were dose dependent (Figure 4G). roClover1 protein was oxidized using 2 mM DPS and displayed a major absorbance peak at 403 nm and a minor shoulder at ~475 nm (Figure 4A). By contrast, when fresh protein was reduced using 5 mM DTT, it displayed a major absorbance peak at 399 nm and a minor shoulder at 505 nm, essentially overlapping with its excitation peak of 507 nm (Figure 4B).

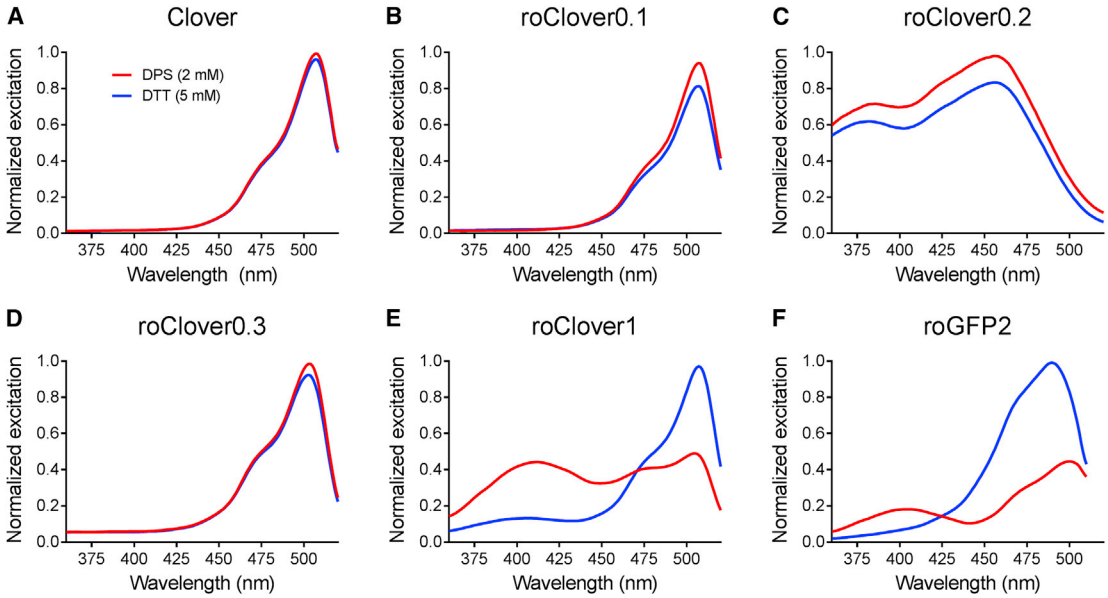

Figure 3. Fluorescence Excitation Spectra of Fluorescent Proteins Exposed to Oxidizer and Reducing Agent

Excitation scans of Clover (A), roClover0.1 (B), roClover0.2 (C), roClover0.3 (D), roClover1 (E), and roGFP2 (F) purified protein after treatment with DPS (2 mM, red trace) or DTT (5 mM, blue trace). Only roClover1 and roGFP2 were redox sensitive.

Interestingly, whereas the neutral chromophore (A band) showed a large excitation peak in the oxidized form, in the reduced form it was greatly diminished, yet the absorbance at ~400 nm decreased by only 20%. The dynamic range of the fully oxidized and reduced roClover1 protein was 6.8 at pH 7.4. As expected, in contrast to roClover1, Clover showed no responses to DPS or DTT (Figure 3A). Since the E222Q mutation is known to slow chromophore maturation (Pouwels et al., 2008), we measured the maturation rate of roClover1 and found that it developed with a time constant ($\tau_{1/2}$) of 22 min, compared with 23 min for EGFP. Clover^{wt} matured approximately 30% faster than both FPs, at 15 min (Figure S2).

Due to the complex spectral properties of roClover1, including the mixture of blue and green emission after excitation of the neutral chromophore (Figures 4A and 4B), we limited our examination of QY and EC values primarily to the minor anionic species, which produces exclusively green emission. The QY of roClover1's anionic chromophore was lower than that of the related GFP-S65G/H203V/E222Q mutant (lacking H148D) (Jung et al., 2005), with ϕ = 0.01–0.02 compared with 0.18 (Table 2). With its larger absorbance ($EC_{400} \approx 30.0$ mM^{-1} cm^{-1}), it is plausible that the roClover1 neutral chromophore would feature a greater QY than the anionic chromophore, but in any case, these values likely set a realistic minimum benchmark for roClover1's brightness compared with other roFPs at physiological pH, which may be prohibitively low in cells but useful for *in vitro* studies and further structure-guided engineering efforts.

We additionally determined the QY and EC of the anionic roGFP1 and roGFP2 chromophore. roGFP1's excitation spectrum predominantly reflected the QY of the oxidized and reduced states (ϕ = 0.40 and 0.71), with a relatively unchanged EC, whereas the QY of the anionic roGFP2 chromophore changed little (ϕ = 0.61 and 0.67) (Table 2). Interestingly, roGFP2's EC can almost entirely account for its dynamic range: the A-band EC increases 2.6-fold upon oxidation (11.0–28.4 mM^{-1} cm^{-1}), while the B-band EC decreases 2.2-fold (50.6–23.1 mM^{-1} cm^{-1}), yielding a 5.7-fold ratio change, practically matching its dynamic range of 5.8–6.0.

Photoactivation of roFPs

We next attempted to photoactivate roClover1 under conditions that produced 10-fold enhancement of the PA-GFP signal and observed a global decrease in absorbance consistent with mild photobleaching, rather than photoactivation (Figure 2F). By comparison, roGFP1 photoactivated with a 5-fold increase in B-band absorbance, with the post-exposure absorbance spectrum revealing a large shift to the anionic chromophore population at the expense of the neutral form (Figure 2G). roGFP2 showed a similar decrease in A-band absorbance to the other FPs but no increase in the B band (Figure 2H). Taken together, the results demonstrate that all mutants featuring S65 were photoactivatable, with PA-GFP and roGFP1 showing the largest effects (10- and 5-fold, respectively), followed by Clover-G65S (2-fold). Mutants with T65 or G65, including roGFP2, Clover, and roClover1, were not photoactivatable. roGFP1 and roGFP2 are based on the wtGFP and EGFP backgrounds, respectively, with roGFP2 featuring EGFP's S65T mutation that stabilizes the anionic chromophore, in contrast to the predominantly neutral chromophore of wtGFP and roGFP1. The ability of roGFP1 to photoactivate is consistent with structural studies of wtGFP and PA-GFP (Brejc et al., 1997; Henderson et al., 2009b) and a report describing strong photoactivation of roGFP1 during confocal imaging (Schwarzländer et al., 2008).

pH Responses of roClover1

roClover1 was more sensitive to pH outside the physiological range than roGFP2, although the B band of both probes was

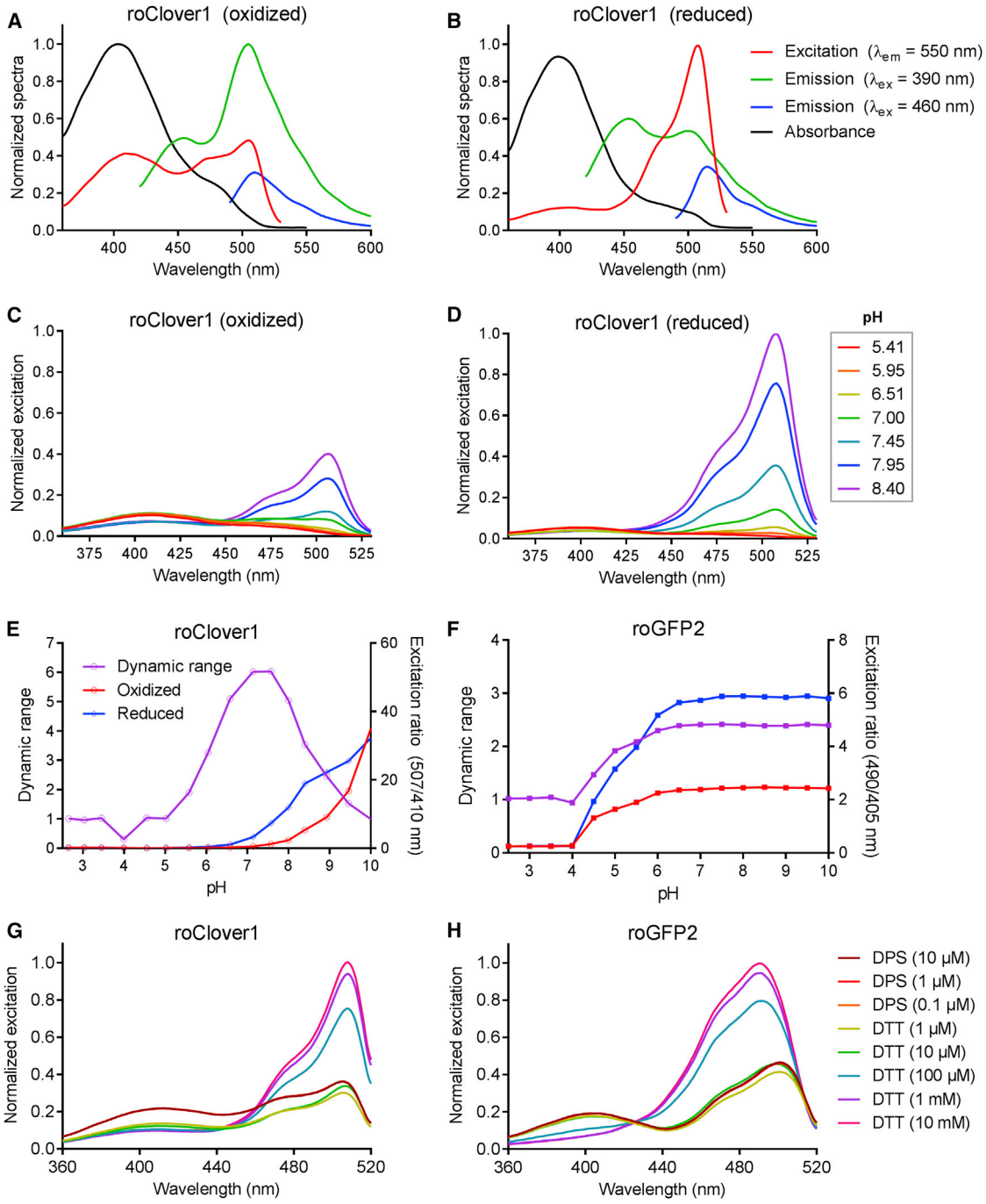

Figure 4. Characterization of roClover1 and roGFP2

(A) roClover1 oxidized with 2 mM DPS.

(B) roClover1 reduced with 5 mM DTT. Excitation spectra (red line) were collected with a detection wavelength of 550 nm. Emission spectra are shown after excitation of the protonated chromophore (A state; green trace, λ_{ex} = 390 nm) and the deprotonated chromophore (B state; blue trace, λ_{ex} = 460 nm). Black trace, absorbance. Data are normalized to the full set of reduced and oxidized protein.

(C and D) Fluorescence excitation spectra of (C) oxidized and (D) reduced roClover1 protein in buffered solutions. Key: pH values. Excitation curves are normalized to the maximum values of the combined oxidized and reduced datasets.

(E and F) pH titration of oxidized and reduced roClover1 protein (E) and roGFP2 (F). "Excitation ratio" is the ratio of fluorescence emission resulting from 410 and 507 nm excitation of the fully reduced and oxidized protein. "Dynamic range" is the quotient of the oxidized and reduced excitation ratios.

(G and H) Fluorescence excitation scans of (G) roClover1 and (H) roGFP2 oxidized with DPS and reduced with DTT. Purified proteins were already fully oxidized under ambient conditions in PBS (pH 7.4), so DPS had little effect (overlapping crimson, red, and orange traces).

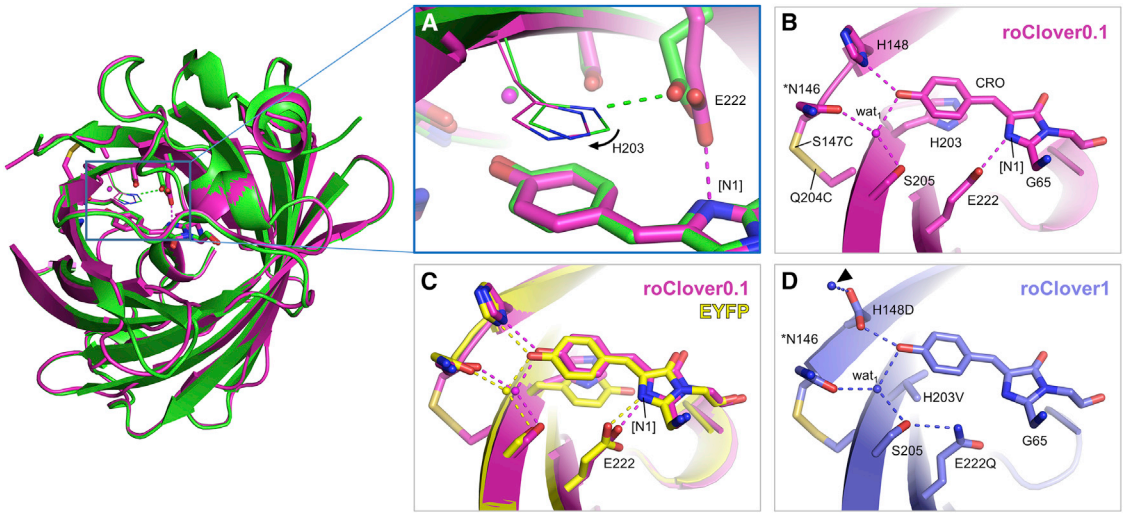

Figure 5. Chromophore Environment and Hydrogen-Bond Network of Redox-Sensitive Clover Mutants

(A) Superposition of Clover (green) and oxidized roClover0.1 (magenta) with arrow indicating the relative direction of H203 movement due to structural strain induced by the C147-C204 disulfide bond. E222 in roClover0.1 forms a hydrogen bond with N1 of the chromophore imidazolinone ring ([N1]) instead of H203.

(B) Hydrogen-bond network of roClover0.1, with disulfide bond visible.

(C) Superposition of roClover0.1 and EYFP structures reveals a similar E222-[N1] hydrogen bond.

(D) H148D in roClover1 is hydrogen bonded to the chromophore phenol and to bulk solvent (black arrowhead). Whereas an S205-Q222 hydrogen bond exists in roClover1, no hydrogen bond is observed between S205 and E222 in roClover0.1. Dashed lines, hydrogen bonds. Asterisk indicates that the N146 main chain only is displayed. Clover, PDB: 5WJ2; roClover0.1, PDB: 5WJ3; roClover1, PDB: 5WJ4; EYFP, PDB: 1YFP.

quenched by acidic conditions. The excitation ratio of the B and A bands rises rapidly above pH 6.0 and plateaus at pH $\geq$ 10 (Figure 4E), demonstrating sensitivity of the anionic chromophore to acidic conditions. Calculating the pK_a using the excitation ratios of the reduced and oxidized proteins separately yields $pK_a > 9$ for both forms. These values are similar to those assigned to the blue/green-emitting mutants GFP-S65T/H148D and GFP-H148D (7.95 and >10.4, respectively) (Shu et al., 2007a). As suggested by the 400 nm absorbance band (Figures 4A and 4B) and positive correlation between fluorescence emission intensity and alkaline pH (Figures 4C and 4D), the roClover1 chromophore is predominantly in the neutral form at pH 7.4. The dynamic range itself was no less than 50% of maximum between pH 6.0 and 8.5 (Figure 4E), although the high pK_a greatly limits its brightness. By comparison, the dynamic range and excitation ratio (B/A) of roGFP2 was very stable between pH 6.0 and 10.0 (Figure 4F). Therefore, the redox responses of roClover1 are susceptible to both acidic and alkaline pH shifts, whereas the redox responses of roGFP2 are susceptible only to acidic pH shifts.

Structure and Properties of roClover0.1

roClover0.1 (Clover-S147C/Q204C) crystallized with the symmetry of space group $P2_12_12_1$ and diffracted to 1.35 Å resolution (Table 1). The crystal structure of roClover0.1, solved by molecular replacement, shows considerable similarity to that of Clover, with an overall RMSD of 0.27 Å. Compared with the Clover structure, the C204-C147 disulfide bond linking β strands 10 and 7 in roClover0.1 shifted the backbone and side chain of H203 ~0.5 Å toward β strand 7 (Figure 5A), placing it further off-center relative to the chromophore phenolate moiety than in Clover and displacing nearby residues such as V150. Consequently, a 1.0 Å outward bulge in β strand 8 is visible around N164 and F165 and is accompanied by a slight rotation of the N146 carbonyl.

The distance between H203 $N_{\delta1}$ and E222 $O_{\varepsilon1}$ in roClover0.1 extends to 3.8 Å, compared with 2.7 Å in Clover, while E222 remains out of H-bond distance to S205 O_γ (4.4–4.9 Å). Instead, E222 $O_{\varepsilon1}$ forms a 2.8 Å hydrogen bond with N1 of the chromophore imidazolinone ring (Figures 5A and 5B), which likely allows it to stay neutral and protonated, thus supporting the deprotonated chromophore, as in Clover. The EYFP structure (PDB: 1YFP) reveals a similar conformation of E222 with bond distances to the same atoms within 0.1–0.2 Å (Wachter et al., 1998), suggesting that the S65G substitution allows E222 to occupy space vacated by loss of the S65/T65 hydroxyl side chain in both roClover0.1 and EYFP (Figure 5C). Overall, these interactions break up the proton wire that normally stabilizes the neutral A state of GFPs and shifts the thermodynamic equilibrium of roClover0.1 toward the anionic B state, just as in Clover. The excitation and emission maxima of Clover and roClover0.1 are nearly identical (Table 2).

We determined the QY (ϕ) and EC (ε) of roClover0.1, yielding $\phi = 0.79$ for the oxidized form, which is among the largest values for a GFP to date and identical to that of PA-GFP_{on}, just surpassing that of mClover3 ($\phi = 0.78$) (Bajar et al., 2016). The EC of roClover0.1_{ox} matched that of $Clover^{wt}$ with ε_{505} of 96,000 M^{-1} cm^{-1}, while that of roClover0.1_{rd} was slightly lower at 86,600 M^{-1} cm^{-1}, with $\phi = 0.75$, identical to the QY of $Clover^{wt}$ (Table 2). The ε_{400} values for the minor roClover0.1 A band were 7,900 and 11,760 M^{-1} cm^{-1} for the oxidized and reduced forms, respectively, showing an inverse relationship with the ε_{505} values, consistent with roClover0.1's very slight ratiometric behavior ($\delta < 2$).

Structure of roClover1

roClover1 crystallized in its oxidized form with symmetry of space group $P4_32_12$ and diffracted to 1.6 Å resolution (Table 1). The π-π stacking interaction between H203 and the chromophore of Clover is disrupted due to H203V. Unlike the GFP-S65T/H148D mutant (Shu et al., 2007a), roClover1 features Gln at position 222, which is a much poorer proton acceptor than Glu. The Q222 $N_{\varepsilon 2}$ is 3.1 Å from S205 O_{γ} and Q222 $O_{\varepsilon 1}$ is 2.8–2.9 Å from two proximal water molecules trapped within the protein. Together these H bonds likely stabilize the orientation of Q222. We observe the same structural water (wat_1) hydrogen bonded to the chromophore and the N146 backbone carbonyl and S205 (Figure 5D), as in EGFP and all Clover variants described here.

The roClover1 chromophore shows striking deviations from planarity compared with roClover0.1 (Table S2), with the roClover1 chromophore phenol moiety oriented directly toward the D148 side chain, which is only 2.5–2.7 Å away (Figure 5D). The conspicuous orientation and minimal distance to D148 suggest a short, strong H bond similar to that observed in the crystal structure of GFP-S65T/H148D, which also showed a similar deviation from planarity that was pH dependent (Shu et al., 2007a). This interaction, as well as the prominent ~400 nm absorbance peak (Figures 4A and 4B), implies that the roClover1 chromophore is predominantly in the neutral phenol form at physiological pH, and the proximal D148 serves as a proton acceptor whose efficiency is likely modulated by geometric strain induced by C147-C204 disulfide bond formation. Solvent accessibility may account for the pH sensitivity of roClover1, as H148D appears to be hydrogen bonded to a chain of water molecules leading directly to the protein surface (Figure 5D).

DISCUSSION

We have produced a crystal structure of the bright GFP, Clover, and described critical structural features that distinguish it from EGFP. Using the Clover crystal structure, we rationally designed, crystallized, and solved the structures of a redox-sensitive mutant, roClover1, and its parental template, roClover0.1 (Clover-S147C/Q204C). We begin by discussing features of Clover that contribute to its optical characteristics and detail the interactions that perturbed the chromophore to the predominantly anionic form. We continue by examining the performance of roClover1 as a redox sensor that functions through a proton acceptor mechanism different from that of the roGFPs.

Several features appear to contribute to the high QY of Clover, including a reduction in non-radiative decay pathways, rigorous chromophore deprotonation that suppresses the neutral chromophore species and conformationally restricts E222, and a restructuring of the H-bond network in Clover's ground state that may reduce the energetic barrier to excited-state transition.

Reduction in Non-radiative Decay Pathways

Greater chromophore packing and the π-π stacking interaction provided by the bulky T203H substitution in Clover decrease the chromophore's conformational freedom and hold it more rigidly in place, thereby decreasing the likelihood of non-radiative de-excitation. The larger histidine may also exclude solvent more rigorously than the smaller threonine. In addition, the stacking interaction likely opposes *cis-trans* isomerization and photochromic behavior, which are important pathways of non-radiative decay (Jung et al., 2005). Single-bond rotation of the phenolate group around the methylene bridge relative to the imidazolinone moiety may still be possible, as suggested in a recent study of Clover (Bajar et al., 2016), although it is unclear whether the π-π stacking interaction would limit this motion.

Similarity of Clover's Hydrogen-Bond Network to the Excited EGFP I* State

The T203H mutation potentially improves Clover's QY by making the ground-state H-bond network more similar to that observed in the transient, highly fluorescent I* form. T203 appears to be responsible in EGFP for the ~470 nm vibronic shoulder that is visible in the B-state configuration but not observed in the I* form (Lam et al., 2012). There, T203 is rotated away from the phenolate group and cannot contribute an H bond (Brejc et al., 1997). The same H-bond partners present in the EGFP I* form are present in the Clover ground state, as revealed by our crystal structure. The S65G/T203H mutation pair in Clover results in an H-bond network reminiscent of both the B- and the I-states, but not identical to either (Figure 1A). Our observations are consistent with the hypothesis proposed in the original study (Lam et al., 2012) that disrupting the T203-chromophore H bond improves QY by removing a potentially important pathway for non-radiative decay of the excited state. The T203H mutation may eliminate the energetic cost of T203 side-chain rotation upon excitation, thereby streamlining the electronic transition to the fluorescent excited state. Clover's chromophore did not appear any more or less planar than that of EGFP or sfGFP, and therefore a change in planarity does not contribute to its brightness (Table S2).

Lack of Centrosymmetry

A final property that may contribute to Clover's high QY is the presence of an asymmetric π-stacking center. The T203Y mutation that contributes to yellow emission in *A. victoria* FPs produces a centrosymmetric inversion center that may limit the QY of EYFP (De Meulenaere et al., 2013) (Figure S1A). The EYFP-Y203F mutant showed a QY improvement from 0.60 to 0.76 (De Meulenaere et al., 2013), approaching the maximum range that has been achievable to date for a tyrosine-containing chromophore (Bajar et al., 2016). It is possible that the asymmetric aromatic stacking configuration in Clover (Figure S1B) supports the high QY by influencing its environmental polarizability, although such effects likely involve concerted interactions among residues, as some bright YFPs like citrine (EYFP-Q69M) do have a high QY (0.77) with Y203 (Griesbeck et al., 2001). The Q69A mutation in Clover was reported to improve photostability (Lam et al., 2012), but whether or not it contributes to hyperpolarizability or QY is unclear. PA-GFP_{on}, which retains the wild-type Q69, has a QY nearly equal to that of Clover (Table 2).

Bathochromic Shift

Clover's stacking interaction is also important for Clover's bathochromic shift relative to EGFP. In EYFP and diverse red fluorescent proteins (RFPs), including mGrape3, E2-Crimson, and TagRFP657, a stacked tyrosine extends the emission

wavelength by effectively serving as a polarizable solvent that reduces the energetic gap between the ground and the excited states of the fluorophore (Ng and Lin, 2016; Wachter et al., 1998). Similarly, the *Zoanthus* YFP zFP538 features a π-π stacking interaction between the chromophore and a His rather than a Tyr, and this contributes to its extended emission wavelength (Remington et al., 2005) (Figure S1C). A similar ring-stacking configuration with a neutral H203 contributes to the bathochromic shift of PA-GFP$_{on}$ (Henderson et al., 2009b), which is very structurally similar to Clover (Figure 1D).

We propose that H203 is neutral in Clover because a cationic histidine would blue shift the emission spectrum by withdrawing electron density from the imidazolinone toward the phenolate moiety, effectively increasing the energetic gap between the ground and the excited states. This type of cation interaction is important in the teal FP mTFP1 and cyan amFP486, which both feature a stacked histidine, further suggesting that electron-donating groups around the chromophore phenolate induce a hypsochromic shift (Ai et al., 2006, 2008; Subach and Verkhusha, 2012). Conversely, in the far-red mKate, H197R (203 by EGFP numbering) specifically disrupts a cation-π interaction and moves positive charge density away from the phenolate, thereby producing the bathochromic shift (Ng and Lin, 2016; Shcherbo et al., 2007).

The second contributing factor to Clover's bathochromic shift is the loss of one H bond to the chromophore due to T203H, which in PA-GFP$_{on}$, has been suspected to reduce local stabilization of the phenolate anion and promote greater charge delocalization across the π-electron cloud of the chromophore (Henderson et al., 2009b). Clover's anionic chromophore is stabilized by the same two H bonds as those in PA-GFP$_{on}$, which differ positionally by less than 0.1 Å (Figure 1D). In a sense, Clover, and especially roClover0.1$_{ox}$ (ϕ = 0.79), may effectively mimic a "constitutively activated" PA-GFP (ϕ_{Clover} = 0.76 $\approx$ $\phi_{PA\text{-}GFP}$ = 0.79), but with a far larger EC.

Basis for Clover's Large Extinction Coefficient

We account for the larger EC in Clover on the basis of its absorbance spectrum and its crystal structure. Both the Clover and the roClover0.1 structures indicate a single conformation of E222 that can be superimposed with the major (70%) conformer in EGFP (Figure 1C). Since that conformation is the most conducive for stabilizing the anionic chromophore (Arpino et al., 2012), it follows that Clover should display a greater B-band absorbance consistent with this equilibrium shift and should therefore also feature a larger EC at that wavelength, which is exactly what is observed. The Clover-G65S mutant, with its large neutral chromophore population, represents the contrapositive case, having an EC nearly 40 times lower at 505 nm than Clover (Table 2).

Lack of Photoactivation in Clover

It is Clover's strong equilibrium disfavoring the neutral chromophore that opposes photoactivation. Structural studies have demonstrated that mutations favoring the A state promote photodecarboxylation of *A. victoria* FPs (Henderson et al., 2009b; Patterson and Lippincott-Schwartz, 2002). We show here that the proton wire stabilizing the wtGFP A state via resonance is strongly disrupted in Clover due to S65G/T203H. Conversely, the Clover-G65S absorbance spectrum indicated a large neutral chromophore population consistent with restoration of the PA-GFP-like H-bond network, thus enabling photoactivation. It is not clear to us why Clover-G65S photoactivated with less contrast than PA-GFP, but it is possible that effects of Q69A or the superfolder mutations could play a role, since the PA-GFPs described previously still differ from Clover by seven (Patterson and Lippincott-Schwartz, 2002) and five (Henderson et al., 2009b) superfolder mutations in addition to Q69A, mutations that are known to subtly influence numerous side-chain and electrostatic interactions throughout the sfGFP structure (Pédelacq et al., 2006).

It follows that roGFP1 should photoactivate through a similar decarboxylation mechanism to that of wtGFP and PA-GFP due to its large A-band absorbance and very similar proton wire (Cannon and Remington, 2006; Hanson et al., 2004). The dramatic shift toward the anionic state of roGFP1 after 410 nm illumination could not have been due to reactive oxygen species, since we applied no oxidizer or reducing agent. Moreover, the post-exposure absorbance spectrum matches that of the reduced protein, not the oxidized (Figure 2F). The impact of such photoactivation effects may be especially large for probes with a low dynamic range, including most roFPs (average $\delta_{max} \leq 6$), where very small responses are often considered significant. At worst, unrecognized photoactivation could artificially mimic natural phenomena, such as reactive oxygen species quenching, and lead to erroneous interpretations.

Spectral Properties of roClover1

The dominant A-band absorbance of roClover1 and its dual emission peaks suggest that decay of the excited state in this FP is modulated by multiple internal conversion processes. Blue emission in *A. victoria* FPs is thought to be a result of a dramatic slowdown or reduction in ESPT efficiency (Ai et al., 2007; Stoner-Ma et al., 2008) and has been explored through numerous mutations that ultimately disrupt proton transfer to the final acceptor E222, such as H203V, E222Q, S65G, S205A, S205V, and combinations thereof (Erez et al., 2011). Jung et al. (2005) studied the GFP mutant S65G/H203V/E222Q using time-resolved spectroscopy and observed blue or green emission depending on excitation of the neutral or anionic chromophore species ($\sim$390 and 480 nm, respectively). Although characterizing the photophysical decay processes in roClover1 is beyond the scope of this study, we speculate that roClover1 similarly ejects a blue photon after excitation of its A band, excites the blue shoulder of the B band, and ultimately produces green emission. We attribute the blue emission to a modification in ESPT efficiency due to a major redirection of proton transfer toward D148 (2.5–2.7 Å from the chromophore phenol), which is similar what has been characterized in the GFP-S65T/H148D mutant (Oltrogge and Boxer, 2015).

The excitation maxima of roClover0.2 (roClover0.1-H148D) were similar to those of GFP-S65T/H148D (400 and 469 nm) at pH 7.4 (Shu et al., 2007a), although its emission was greatly red shifted to 520 nm, perhaps due to the T203H mutation and the described stacking interaction. Both S65T and S65G reduce the efficiency of proton transfer to E222 in conjunction with H148D. Specifically, S65G relative to wtGFP eliminates an H-bond donor to anionic E222 and increases its conformational freedom, leading to a less stable proton wire where E222 would

be the final H-bond acceptor. We suspect that the short H bond between H148D and the chromophore in GFP-S65T/H148D ($\leq$2.4 Å) and in roClover1 (2.5–2.7 Å) effectively dominates the proton transfer pathway and minimizes the contribution of E222 (or Q222 in Clover1). The ratiometric excitation spectrum of roClover1 and lack of photoactivation support the concept that ratiometric biosensors can be generated by redirecting proton transfer to acceptors other than the canonical E222.

pH Responses of roClover1

The intrinsic pH sensitivity of FPs becomes particularly relevant when considering FP biosensors, since their responses ultimately hinge on the chromophore ionization equilibrium. roGFP-iE, for example, displays large pH-dependent excitation ratio shifts that appear to be a product of increased solvent accessibility afforded by the H148S substitution, among others (Lohman and Remington, 2008). Even the mApple-derived rxRFP1, an intensiometric roFP unrelated to EGFP, has a pK_a of 8.7 (Fan et al., 2015). The high pK_a of many biosensors, including the Ca^{2+} sensors, may be important for allowing ESPT or other functionally important internal conversion processes to occur efficiently near physiological pH (Barnett et al., 2017).

In the case of roClover1, loss of H148 as well as the presence of D148 likely contributes to its pH sensitivity. H148 has been shown to act as a "proton gate" that shields the chromophore from bulk solvent (Shinobu and Agmon, 2015), and replacement with residues such as Gly or Asp has conferred pH sensitivity in other mutants (Bizzarri et al., 2007). In the crystal structures of GFP-S65T/H148D and roClover1, D148 is solvent exposed (Leiderman et al., 2007), which should amplify the effects of environmental pH changes. Despite its low brightness, the dynamic range of roClover1 peaks at pH $\approx$7.4 (δ_{max} = 6.8) with an excitation ratio no less than 50% of δ_{max} between pH 6.0 and 8.5 *in vitro*. Further efforts in roFP development would benefit from optimizing pH-independent performance characteristics and shielding the chromophore from solvent, which might also be achieved through protein domain fusions that couple the chromophore ionization state to structural changes in the fusion partner.

roClover1 is the product of a rational engineering strategy and is a proof-of-concept probe that may inform development of excitation-ratiometric biosensors from FPs that do not naturally undergo proton transfer, a process that appears to be important and perhaps essential for excitation ratiometry (Henderson et al., 2009a). A roClover1-like design strategy could be useful during construction of new ratiometric biosensors, which have potential to overcome the inherent limitations of intensiometric measurement and yield probes with reduced susceptibility to effects of bleaching, variable expression, and environmental influences, which would be self-corrected by excitation ratiometry.

Our study also grants further insight into the redox-independent photoactivation dynamics of roGFP1 and roGFP2, the archetypal roFPs. roClover1 did not photoactivate, despite its predominantly neutral chromophore, while roGFP1 photoactivated strongly under our illumination paradigm. The Clover and Clover-G65S photoactivation data further suggest, in agreement with prior crystallographic work (Henderson et al., 2009b), that the degree to which an avFP that contains E222 can photoactivate is, to a large extent, proportional to the amplitude of its A-band absorbance. We urge caution in the use of roGFP1 at high power intensities, with tightly focused illumination, and in continuous imaging experiments.

On the path to developing the non-photoactivatable excitation-ratiometric redox sensor, roClover1, we crystallized roClover0.1 (Clover-S147C/Q204C) and solved its structure to 1.3 Å resolution. The roClover0.1 structure may suggest a specific chromophore configuration conducive to high QY (ϕ = 0.79), although we cannot rule out the potential involvement of other factors such as dimer interactions. We are currently using roClover0.1 as a template for high-throughput library-based screening of advanced roFPs. The Clover crystal structure itself reveals a modified proton wire as well as other critical atomistic interactions responsible for its high brightness, which we have described. These structural and functional insights may facilitate development of improved biosensors and optical highlighters derived from *A. victoria* and other lineages.

STAR★METHODS

Detailed methods are provided in the online version of this paper and include the following:

- KEY RESOURCES TABLE
- CONTACT FOR REAGENT AND RESOURCE SHARING
- METHOD DETAILS
  - Engineering of Clover Variants
  - Expression and Purification
  - Crystallography
  - Crystallographic Data Collection, Processing, and Refinement
  - Optical Assays
  - Photoactivation of Purified Protein
  - Chromophore Maturation
- QUANTIFICATION AND STATISTICAL ANALYSIS
- DATA AND SOFTWARE AVAILABILITY

SUPPLEMENTAL INFORMATION

Supplemental Information includes two figures and two tables and can be found with this article online at https://doi.org/10.1016/j.str.2017.12.006.

ACKNOWLEDGMENTS

This work is based on research conducted at the GM/CA CAT (GM/CA@APS). GM/CA@APS has been funded in whole or in part with federal funds from the National Cancer Institute (ACB-12002) and the National Institute of General Medical Sciences (AGM-12006). This research used resources of the Advanced Photon Source, a US Department of Energy (DOE) Office of Science User Facility operated for the DOE Office of Science by Argonne National Laboratory under Contract DE-AC02-06CH11357. We thank Samie R. Jaffrey and Manu Sharma (Weill Cornell Medicine) for critical reading of the manuscript. Kevin M. Dean and Lauren M. Barnett provided helpful advice on quantum yield measurements.

AUTHOR CONTRIBUTIONS

C.F.L. and B.C.C. conceptualized the experiments and interpreted results. B.C.C. performed the experiments and wrote the manuscript. C.F.L. solved

and refined the crystal structures. G.A.P. and C.F.L. provided advice and supported the project. All authors edited the manuscript.

Received: September 11, 2017
Revised: October 31, 2017
Accepted: December 6, 2017
Published: January 4, 2018

REFERENCES

Adams, P.D., Afonine, P.V., Bunkoczi, G., Chen, V.B., Davis, I.W., Echols, N., Headd, J.J., Hung, L.W., Kapral, G.J., Grosse-Kunstleve, R.W., et al. (2010). PHENIX: a comprehensive Python-based system for macromolecular structure solution. Acta Crystallogr. D Biol. Crystallogr. *66*, 213–221.

Ai, H., Henderson, J.N., Remington, S.J., and Campbell, R.E. (2006). Directed evolution of a monomeric, bright and photostable version of *Clavularia* cyan fluorescent protein: structural characterization and applications in fluorescence imaging. Biochem. J. *400*, 531–540.

Ai, H.W., Olenych, S.G., Wong, P., Davidson, M.W., and Campbell, R.E. (2008). Hue-shifted monomeric variants of *Clavularia* cyan fluorescent protein: identification of the molecular determinants of color and applications in fluorescence imaging. BMC Biol. *6*, 13.

Ai, H.W., Shaner, N.C., Cheng, Z., Tsien, R.Y., and Campbell, R.E. (2007). Exploration of new chromophore structures leads to the identification of improved blue fluorescent proteins. Biochemistry *46*, 5904–5910.

Arpino, J.A., Rizkallah, P.J., and Jones, D.D. (2012). Crystal structure of enhanced green fluorescent protein to 1.35 a resolution reveals alternative conformations for Glu222. PLoS One *7*, e47132.

Bajar, B.T., Wang, E.S., Lam, A.J., Kim, B.B., Jacobs, C.L., Howe, E.S., Davidson, M.W., Lin, M.Z., and Chu, J. (2016). Improving brightness and photostability of green and red fluorescent proteins for live cell imaging and FRET reporting. Sci. Rep. *6*, 20889.

Barnett, L.M., Hughes, T.E., and Drobizhev, M. (2017). Deciphering the molecular mechanism responsible for GCaMP6m's Ca^{2+}-dependent change in fluorescence. PLoS One *12*, e0170934.

Barondeau, D.P., Putnam, C.D., Kassmann, C.J., Tainer, J.A., and Getzoff, E.D. (2003). Mechanism and energetics of green fluorescent protein chromophore synthesis revealed by trapped intermediate structures. Proc. Natl. Acad. Sci. USA *100*, 12111–12116.

Bindels, D.S., Haarbosch, L., van Weeren, L., Postma, M., Wiese, K.E., Mastop, M., Aumonier, S., Gotthard, G., Royant, A., Hink, M.A., et al. (2016). mScarlet: a bright monomeric red fluorescent protein for cellular imaging. Nat. Methods *14*, 1–12.

Bizzarri, R., Nifosì, R., Abbruzzetti, S., Rocchia, W., Guidi, S., Arosio, D., Garau, G., Campanini, B., Grandi, E., Ricci, F., et al. (2007). Green fluorescent protein ground states: the influence of a second protonation site near the chromophore. Biochemistry *46*, 5494–5504.

Brejc, K., Sixma, T.K., Kitts, P.A., Kain, S.R., Tsien, R.Y., Ormo, M., and Remington, S.J. (1997). Structural basis for dual excitation and photoisomerization of the *Aequorea victoria* green fluorescent protein. Proc. Natl. Acad. Sci. USA *94*, 2306–2311.

Cannon, M.B., and Remington, S.J. (2006). Re-engineering redox-sensitive green fluorescent protein for improved response rate. Protein Sci. *15*, 45–57.

Chalfie, M., Tu, Y., Euskirchen, G., Ward, W.W., and Prasher, D.C. (1994). Green fluorescent protein as a marker for gene expression. Science *263*, 802–805.

Chu, J., Sens, A., Ataie, N., Dana, H., Macklin, J., Laviv, T., Zhang, F., Welf, E.S., Dean, K.M., Baird, M.A., et al. (2016). A bright cyan-excitable orange fluorescent protein enables dual-emission microscopy and highly sensitive bioluminescence imaging in vivo. Nat. Biotechnol. *34*, 760–767.

Cranfill, P.J., Sell, B.R., Baird, M.A., Allen, J.R., Lavagnino, Z., de Gruiter, H.M., Kremers, G.J., Davidson, M.W., Ustione, A., and Piston, D.W. (2016). Quantitative assessment of fluorescent proteins. Nat. Methods *13*, 557–562.

Dooley, C.T., Dore, T.M., Hanson, G.T., Jackson, W.C., Remington, S.J., and Tsien, R.Y. (2004). Imaging dynamic redox changes in mammalian cells with green fluorescent protein indicators. J. Biol. Chem. *279*, 22284–22293.

Emsley, P., and Cowtan, K. (2004). Coot: model-building tools for molecular graphics. Acta Crystallogr. D Biol. Crystallogr. *60*, 2126–2132.

Erez, Y., Gepshtein, R., Presiado, I., Trujillo, K., Kallio, K., Remington, S.J., and Huppert, D. (2011). Structure and excited-state proton transfer in the GFP S205A mutant. J. Phys. Chem. B *115*, 11776–11785.

Fan, Y., Chen, Z., and Ai, H.W. (2015). Monitoring redox dynamics in living cells with a redox-sensitive red fluorescent protein. Anal. Chem. *87*, 2802–2810.

Griesbeck, O., Baird, G.S., Campbell, R.E., Zacharias, D.A., and Tsien, R.Y. (2001). Reducing the environmental sensitivity of yellow fluorescent protein. J. Biol. Chem. *276*, 29188–29194.

Hanson, G.T., Aggeler, R., Oglesbee, D., Cannon, M., Capaldi, R.A., Tsien, R.Y., and Remington, S.J. (2004). Investigating mitochondrial redox potential with redox-sensitive green fluorescent protein indicators. J. Biol. Chem. *279*, 13044–13053.

Henderson, J.N., Osborn, M.F., Koon, N., Gepshtein, R., Huppert, D., and Remington, S.J. (2009a). Excited state proton transfer in the red fluorescent protein mKeima. J. Am. Chem. Soc. *131*, 13212–13213.

Henderson, J.N., Gepshtein, R., Heenan, J.R., Kallio, K., Huppert, D., and Remington, S.J. (2009b). Structure and mechanism of the photoactivatable green fluorescent protein. J. Am. Chem. Soc. *131*, 4176–4177.

Huber, R.G., Margreiter, M.A., Fuchs, J.E., Von Grafenstein, S., Tautermann, C.S., Liedl, K.R., and Fox, T. (2014). Heteroaromatic pi-stacking energy landscapes. J. Chem. Inf. Model. *54*, 1371–1379.

Jung, G., Wiehler, J., and Zumbusch, A. (2005). The photophysics of green fluorescent protein: influence of the key amino acids at positions 65, 203, and 222. Biophys. J. *88*, 1932–1947.

Kredel, S., Oswald, F., Nienhaus, K., Deuschle, K., Röcker, C., Wolff, M., Heilker, R., Nienhaus, G.U., and Wiedenmann, J. (2009). mRuby, a bright monomeric red fluorescent protein for labeling of subcellular structures. PLoS One *4*, 1–7.

Lam, A.J., St-Pierre, F., Gong, Y., Marshall, J.D., Cranfill, P.J., Baird, M.A., McKeown, M.R., Wiedenmann, J., Davidson, M.W., Schnitzer, M.J., et al. (2012). Improving FRET dynamic range with bright green and red fluorescent proteins. Nat. Methods *9*, 1005–1012.

Leiderman, P., Genosar, L., Huppert, D., Shu, X., Remington, S.J., Solntsev, K.M., and Tolbert, L.M. (2007). Ultrafast excited-state dynamics in the green fluorescent protein variant S65T/H148D. 3. Short- and long-time dynamics of the excited-state proton transfer. Biochemistry *46*, 12026–12036.

Lohman, J.R., and Remington, S.J. (2008). Development of a family of redox-sensitive green fluorescent protein indicators for use in relatively oxidizing subcellular environments. Biochemistry *47*, 8678–8688.

Magde, D., Wong, R., and Seybold, P.G. (2002). Fluorescence quantum yields and their relation to lifetimes of Rhodamine 6G and fluorescein in nine solvents: improved absolute standards for quantum yields. Photochem. Photobiol. *75*, 327–334.

McCoy, A.J., Grosse-Kunstleve, R.W., Adams, P.D., Winn, M.D., Storoni, L.C., and Read, R.J. (2007). Phaser crystallographic software. J. Appl. Crystallogr. *40*, 658–674.

Meech, S.R. (2009). Excited state reactions in fluorescent proteins. Chem. Soc. Rev. *38*, 2922–2934.

De Meulenaere, E., Nguyen Bich, N., De Wergifosse, M., Van Hecke, K., Van Meervelt, L., Vanderleyden, J., Champagne, B., and Clays, K. (2013). Improving the second-order nonlinear optical response of fluorescent proteins: the symmetry argument. J. Am. Chem. Soc. *135*, 4061–4069.

Ng, H.L., and Lin, M.Z. (2016). Structure-guided wavelength tuning in far-red fluorescent proteins. Curr. Opin. Struct. Biol. *39*, 124–133.

Oltrogge, L.M., and Boxer, S.G. (2015). Short hydrogen bonds and proton delocalization in green fluorescent protein (GFP). ACS Cent. Sci. *1*, 148–156.

Otwinowski, Z., and Minor, W. (1997). Processing of X-ray diffraction data collected in oscillation mode. Methods Enzymol. *276*, 307–326.

Patterson, G.H., and Lippincott-Schwartz, J. (2002). A photoactive GFP for selective photolabeling of proteins and cells. Science *297*, 1873–1877.

Pédelacq, J.D., Cabantous, S., Tran, T., Terwilliger, T.C., and Waldo, G.S. (2006). Engineering and characterization of a superfolder green fluorescent protein. Nat. Biotechnol. *24*, 79–88.

Pouwels, L.J., Zhang, L., Chan, N.H., Dorrestein, P.C., and Wachter, R.M. (2008). Kinetic isotope effect studies on the de novo rate of chromophore formation in fast- and slow-maturing GFP variants. Biochemistry *47*, 10111–10122.

Remington, S.J., Wachter, R.M., Yarbrough, D.K., Branchaud, B., Anderson, D.C., Kallio, K., and Lukyanov, K.A. (2005). zFP538, a yellow-fluorescent protein from *Zoanthus*, contains a novel three-ring chromophore. Biochemistry *44*, 202–212.

Sarkisyan, K.S., Goryashchenko, A.S., Lidsky, P.V., Gorbachev, D.A., Bozhanova, N.G., Gorokhovatsky, A.Y., Pereverzeva, A.R., Ryumina, A.P., Zherdeva, V.V., Savitsky, A.P., et al. (2015). Green fluorescent protein with anionic tryptophan-based chromophore and long fluorescence lifetime. Biophys. J. *109*, 380–389.

Schwarzländer, M., Fricker, M., Müller, C., Marty, L., Brach, T., Novak, J., Sweetlove, L., Hell, R., and Meyer, A.J. (2008). Confocal imaging of glutathione redox potential in living plant cells. J. Microsc. *231*, 299–316.

Schwede, T., Kopp, J., Guex, N., and Peitsch, M.C. (2003). SWISS-MODEL: an automated protein homology-modeling server. Nucleic Acids Res. *31*, 3381–3385.

Shcherbo, D., Merzlyak, E.M., Chepurnykh, T.V., Fradkov, A.F., Ermakova, G.V., Solovieva, E.A., Lukyanov, K.A., Bogdanova, E.A., Zaraisky, A.G., Lukyanov, S., et al. (2007). Bright far-red fluorescent protein for whole-body imaging. Nat. Methods *4*, 741–746.

Shi, X., Abbyad, P., Shu, X., Kallio, K., Kanchanawong, P., Childs, W., Remington, S.J., and Boxer, S.G. (2007). Ultrafast excited-state dynamics in the green fluorescent protein variant S65T/H148D. 2. Unusual photophysical properties. Biochemistry *46*, 12014–12025.

Shinobu, A., and Agmon, N. (2015). The hole in the barrel: water exchange at the GFP chromophore. J. Phys. Chem. B *119*, 3464–3478.

Shu, X., Kallio, K., Shi, X., Abbyad, P., Kanchanawong, P., Childs, W., Boxer, S.G., and Remington, S.J. (2007a). Ultrafast excited-state dynamics in the green fluorescent protein variant S65T/H148D 1. Mutagenesis and structural studies. Biochemistry *46*, 12005–12013.

Shu, X., Leiderman, P., Gepshtein, R., Smith, N.R., Kallio, K., Huppert, D., and Remington, S.J. (2007b). An alternative excited-state proton transfer pathway in green fluorescent protein variant S205V. Protein Sci. *16*, 2703–2710.

Stoner-Ma, D., Jaye, A.A., Ronayne, K.L., Nappa, J., Tonge, P.J., and Meech, S.R. (2008). Ultrafast electronic and vibrational dynamics of stabilized A state mutants of the green fluorescent protein (GFP): snipping the proton wire. Chem. Phys. *350*, 193–200.

Subach, F.V., and Verkhusha, V.V. (2012). Chromophore transformations in red fluorescent proteins. Chem. Rev. *112*, 4308–4327.

Subach, O.M., Cranfill, P.J., Davidson, M.W., and Verkhusha, V.V. (2011). An enhanced monomeric blue fluorescent protein with the high chemical stability of the chromophore. PLoS One *6*, e28674.

Thorn, K. (2017). Genetically encoded fluorescent tags. Mol. Biol. Cell *28*, 848–857.

Wachter, R.M., Elsliger, M., Kallio, K., Hanson, G.T., and Remington, S.J. (1998). Structural basis of spectral shifts in the yellow-emission variants of green fluorescent protein. Structure *6*, 1267–1277.

STAR★METHODS

KEY RESOURCES TABLE

REAGENT or RESOURCE	SOURCE	IDENTIFIER
Bacterial and Virus Strains		
Escherichia coli BL21(DE3)	Petsko lab	N/A
Escherichia coli DH5α	Petsko lab	N/A
Chemicals, Peptides, and Recombinant Proteins		
TEV protease	Life Technologies	Cat#: 10127-017
Pfu polymerase	Agilent	Cat#: 600153
HisPur Cobalt Resin	Thermo Scientific	Cat#: PI89966
Dithiothreitol (DTT)	GoldBio	Cat#: DTT100; CAS: 3483-12-3
Aldrithiol-2 (2,2-dipyridyl disulfide; DPS)	Sigma-Aldrich	Cat#: 143049; CAS: 2127-03-9
Invitrogen Magic Media *E. coli* expression medium	Thermo Scientific	Cat#: K6810
Fluorescein	Sigma-Aldrich	Cat#: 32615
Deposited Data		
Clover (structure and coordinates)	This work	PDB: 5WJ2
roClover0.1 (structure and coordinates)	This work	PDB: 5WJ3
roClover1 (structure and coordinates)	This work	PDB: 5WJ4
Recombinant DNA		
pcDNA3.1-Clover-mRuby2	Beam Lab, unpublished plasmids	Addgene #49089; (Lam et al., 2012)
roGFP1	Remington Lab, University of Oregon	N/A
roGFP2	Remington Lab, University of Oregon	N/A
PA-GFP	Richard Youle lab	Addgene #23348
pET28a-empty (thrombin site replaced with TEV)	Petsko lab	N/A
pET28a-roClover0.1 (His_6-tagged with TEV site)	This work	N/A
pET28a-roClover1 (His_6-tagged with TEV site)	This work	N/A
Software and Algorithms		
GraphPad Prism 6	GraphPad Software, Inc.	https://www.graphpad.com/
Swiss-Model	(Schwede et al., 2003)	https://swissmodel.expasy.org/
Phaser	(McCoy et al., 2007)	http://www-structmed.cimr.cam.ac.uk/phaser_obsolete/
PHENIX	(Adams et al., 2010)	https://www.phenix-online.org/
Coot	(Emsley and Cowtan, 2004)	https://www2.mrc-lmb.cam.ac.uk/personal/pemsley/coot/
HKL2000	(Otwinowski and Minor, 1997)	http://www.hkl-xray.com/download-instructions-hkl-2000
Other		
Ultra-Violet (UV) High Power LED Star (400-410 nm)	LED Supply	Cat#: A008-UV400-65
BioCell 1 cm Quartz Vessel	Biotek	Cat#: 7272051
Hellma Fluorescence Cuvette, Ultra Micro	Sigma-Aldrich	Cat#: Z802549
96-well Clear Bottom Black Polystyrene Microplates	Corning	Cat#: 3631

CONTACT FOR REAGENT AND RESOURCE SHARING

Further information and requests for reagents should be directed to and will be fulfilled by the lead contact, Ce Feng Liu (cel2010@med.cornell.edu).

METHOD DETAILS

Engineering of Clover Variants

Clover was PCR amplified from pcDNA3.1-Clover-mRuby2 (Addgene #49089) using primers containing *Nde*I/*Xho*I restriction sites and cloned into a pET28a expression vector containing a TEV-cleavable N-terminal His_6-tag. Site-directed mutagenesis was performed on pET28a-Clover using the QuikChange (Stratagene) method, DNA was transformed into DH5α competent cells, and mutations were confirmed by sequencing (Macrogen).

Expression and Purification

Fluorescent protein was expressed in 500 mL MagicMedia (Invitrogen) using *E. coli* strain BL21(DE3) at 18°C for 36 hr. Frozen pellets were thawed, sonicated, and clarified by centrifugation. Soluble protein was isolated using HisPur Co^{2+} resin (Thermo Scientific) according to manufacturer instructions. To the extent possible, all proteins were protected from light and kept on ice during purification. Cleavage of the His_6-tag was performed during dialysis into PBS using His_6-TEV protease at 4°C overnight. The cleaved tag and TEV protease were removed by adsorption onto fresh Co^{2+} resin and the pure protein flow-through was concentrated to ~30 mg/ml using Amicon centrifugal filter units (EMD-Millipore).

Crystallography

Clover was crystallized by the hanging drop vapor diffusion method using Hampton Research VDX 24-well plates. Typically, 2 μl of 30 mg/mL Clover protein mixed with 2 μl of 1.6 M sodium citrate dihydrate pH 6.5 ("mother liquor") was sealed over a well containing 0.5 mL mother liquor. Crystals in the form of needle clusters appeared in approximately 7 days at 18°C. Individual needle-shaped crystals were dissected from the clusters, looped, and cryoprotected using 15% ethylene glycol in mother liquor.

roClover0.1 (TEV-cleaved) and roClover1 were crystallized by the same method described above except the mother liquor consisted of 100 mM Tris pH 8.5, 25% PEG 3350, and 50 mM $MgCl_2$. Rod-like crystal formation was apparent within 15 min at room temperature for roClover0.1, and 7 days at 18°C for roClover1.

Attempts to reduce roClover0.1 and roClover1 by soaking the crystals in mother liquor containing cryoprotectant (15% ethylene glycol) and fresh DTT were not successful. Crystallographic data collected from all crystals that formed in the presence of 5 mM DTT yielded only the oxidized structures.

Crystallographic Data Collection, Processing, and Refinement

Crystallographic data were collected at GM/CA CAT 23-IDB of the Advanced Photon Source at Argonne National Laboratory. Diffraction data were collected using 0.98 Å wavelength X-rays at 100 K on a Mar225 CCD detector (MarUSA) and processed with program HKL2000 (Otwinowski and Minor, 1997). A homology model of Clover was generated from the crystal structure of an EGFP mutant (PDB: 1QYQ) (Barondeau et al., 2003) using the online server Swiss-Model (Schwede et al., 2003). This homology model was used as a molecular replacement search model and yielded a solution with the program Phaser (McCoy et al., 2007). The initial molecular replacement solution was subjected to multiple rounds of maximum likelihood restrained refinement using PHENIX (Adams et al., 2010) and manual rebuilding with Coot (Emsley and Cowtan, 2004). Complete data collection and refinement statistics are given in Table 1.

Optical Assays

Optical assays were performed using a BioTek Synergy H1 microplate reader in black clear-bottom 96-well assay plates (Corning Costar) or on the BioTek Take3 microplate loaded with a 1 cm pathlength quartz cuvette (BioTek BioCell or Hellma Suprasil). Spectral scans of oxidized and reduced protein were performed by diluting pure protein (1 μM) into 100 μl PBS pH 7.4 supplemented with 2,2-dipyridyl disulfide (Sigma) or dithiothreitol (Fisher Scientific) to final concentrations of 2 mM and 5 mM, respectively, and incubated for 10 min before scanning. We define the excitation ratio of roClover1 as the ratio of the 507 nm to 410 nm peak. Dynamic range of the protein is the quotient of the oxidized and reduced excitation ratios after background subtraction. Optical assays were performed in triplicate with 1 nm step size. Traces represent the average with error bars omitted for readability.

pH sensitivity was assessed using a protocol described previously (Subach et al., 2011). Briefly, FPs (1 μM) were incubated at room temperature (25-27°C) in a series of buffers containing 300 mM NaCl with the addition of 100 mM NaOAc for pH 2.5-5.0 and 100 mM NaH_2PO_4 for pH 4.5-10.0, respectively, for 15 min before analysis. Extinction coefficients were determined using the alkali denaturation method precisely as described (Cranfill et al., 2016).

Quantum yields were determined using λ_{ex} = 460 nm on a PTI QuantaMaster and λ_{det} = 475-650 nm in 1 nm steps. Fluorescein in 0.1 M NaOH (ϕ = 0.925) (Magde et al., 2002) and Clover in PBS (ϕ = 0.76) were cross-referenced as standards for all samples (error was within 3% of literature values for each standard), and integrated intensities of triplicate samples at identical final

absorbance (A_{460} = 0.005) were computed using GraphPad Prism software. For complete oxidation and reduction of roFPs, measurements were taken 10 min after addition of 0.1 mM DPS or 1 mM DTT carried in DMSO ($C_f \leq 0.5\%$).

Photoactivation of Purified Protein

Purified protein (~20 μM) in PBS pH 7.4 was loaded into a fully transparent 1 cm pathlength quartz cuvette and exposed for 20 min to unfocused illumination from a 400-410 nm LED (SemiLED UV) suspended 1 cm above the cuvette. The enclosure was actively fan-cooled to $\leq$ 37°C. Absorbance measurements were performed before and after exposure with blanks subtracted. Stable power output of 14 mW/cm^2 at the cuvette surface was measured using a ThorLabs PM100D power meter equipped with an S130VC high-sensitivity photodetector. Traces represent the average of duplicate experiments with error <10%.

Chromophore Maturation

Individual *E. coli* BL21(DE3) colonies containing the pET28a plasmids were grown in SOC medium (20% glucose) plus kanamycin in round-bottom culture tubes at 37°C aerobically with shaking. After $\geq$12 hours of growth, cultures were pelleted in 2 mL microcentrifuge tubes, resuspended and filled to the brim with 2.2 mL hypoxic expression medium (LB with kanamycin and 5 mM IPTG, roughly degassed by bubbling N_2), and sealed using airtight screw caps with rubberized O-rings. After 3-4 hr of hypoxic growth at 37°C without shaking, cultures were cooled to $\leq$4°C on ice, pelleted, resuspended in ice-cold PBS, and rapidly sonicated on ice. Lysate was clarified by centrifugation at 4°C and diluted serially into room temperature PBS in an air-exposed 96-well black clear-bottom plate. Measurements were immediately taken using a Biotek Synergy H1 microplate reader pre-heated to 37°C and configured for kinetic endpoint scanning with $\lambda_{ex}/\lambda_{em}$ = 495/525 nm at 2 min intervals. Duplicate experiments were averaged after baseline subtraction at t = 0 min and graphed with sigmoidal curve-fitting ($R^2 > 0.97$) using GraphPad Prism software. Maturation half-time ($t_{1/2}$) is the time at which the sample reaches 50% of maximum fluorescence. Total time from unsealing tubes to microplate scanning was always $\leq$10 min.

QUANTIFICATION AND STATISTICAL ANALYSIS

Details regarding statistical and experimental replicates can be found within the Method Details section and/or the corresponding figure legends where appropriate. GraphPad Prism 6 was used for all graphing purposes and analyses. Curve fitting for the maturation assay was performed using the sigmoidal non-linear regression function that is typically used for EC50 determination.

DATA AND SOFTWARE AVAILABILITY

Atomic coordinates and structures have been deposited in the Protein Data Bank under accession codes 5WJ2 (Clover), 5WJ3 (roClover0.1), and 5WJ4 (roClover1).